Electronic Supplementary Material (ESI) for Inorganic Chemistry Frontiers.

SUPPORTING INFORMATION

Broad-range spin-crossover modulation in guest-responsive 2D Hofmann-type coordination polymers

A. Orellana-Silla, R. Turo-Cortés, V. Rubio-Giménez, C. Bartual-Murgui, R. Ameloot, C. Martí-Gastaldo, M. C. Muñoz and J. A. Real

Contents

Experimental section

Materials

All reagents and solvents used were obtained from commercial sources and used as received without further purification.

Synthetic procedure

Single crystals of {Fe(5-OHPym)$_2$[Pt(CN)$_4$]}·H$_2$O and {Fe(5-OHPym)$_2$[Pd(CN)$_4$]}·H$_2$O (**1(OH)^{Pt}·H$_2$O** and **1(OH)^{Pd}·H$_2$O**) were grown by slow liquid-liquid diffusion in a double H-shaped tube. A small amount of Fe(BF)$_4$·6H$_2$O (33.7 mg, 0.1 mmol) was deposited on one side while the other positions were occupied by the 5-hydroxipyrimidine ligand (20.0 mg, 0.2 mmol) and K$_2$[Pd(CN)$_4$] or K$_2$[Pt(CN)$_4$] (34.1 mg or 43.1 mg, 0.1 mmol). The tube was filled with H$_2$O (*ca.* 10 mL), sealed and leaved undisturbed for 4 weeks obtaining plate single crystals in 70% yield. Elemental analysis: Calculated for **1(OH)^{Pt}·H$_2$O** [C$_{12}$H$_{10}$FeN$_8$O$_3$Pt (565.18) (%)]: C 25.50, H 1.78, N 19.83 Found (%): C 25.29, H 1.84, N 20.07; Calculated for **1(OH)^{Pd}·H$_2$O** [C$_{12}$H$_{10}$FeN$_8$O$_3$Pd (476.52) (%)]: C 30.25, H 2.12, N 23.51 Found (%): C 30.12, H 2.04, 23.69.

1(OH)^{Pt} and **1(OH)^{Pd}** desolvated compounds were obtained by introducing crystals of **1(OH)^{Pt}·H$_2$O** and **1(OH)^{Pd}·H$_2$O** in an oven at 400 K for 30 minutes. **1(OH)^{Pt}·xMeOH**, **1(OH)^{Pd}·xMeOH**, **1(OH)^{Pt}·xEtOH** and **1(OH)^{Pd}·xEtOH** were achieved by submerging freshly prepared **1(OH)^{Pt}** and **1(OH)^{Pd}** in a bath of the corresponding solvent for different times. In all cases the compounds are yellow plate crystals at room temperature and turn red upon cooling at 120K. Elemental analysis: Calculated for **1(OH)^{Pt}·MeOH** [C$_{13}$H$_{12}$FeN$_8$O$_3$Pt (579.21) (%)]: C 26.96, H 2.09, N 19.35 Found (%): C 26.74, H 1.96, N 19.46; Calculated for **1(OH)^{Pd}·MeOH** [C$_{13}$H$_{12}$FeN$_8$O$_3$Pd (490.55) (%)]: C 31.83, H 2.47, N 22.84 Found (%): C 31.86, H 2.49, N 22.78; Calculated for **1(OH)^{Pt}·0.8EtOH** [C$_{13.6}$H$_{12.8}$FeN$_8$O$_{2.8}$Pt (584.03) (%)]: C 27.97, H 2.21, N 19.19 Found (%): C 28.11, H 2.14, N 19.03; Calculated for **1(OH)^{Pd}·0.5EtOH** [C$_{13}$H$_{11}$FeN$_8$O$_{2.5}$Pt (481.55) (%)]: C 32.43, H 2.30, N 23.27 Found (%): C 32.22, H 2.43, N 23.45. E.A. of **1(OH)^{Pt}** and **1(OH)^{Pd}** could not be performed due to the rapidity that they adsorb water from air moisture during sample preparation.

Physical characterization

Elemental analyses (C, H, N) were performed with a CE Instruments EA 1110 CHNS Elemental analyzer.

Magnetic measurements were performed with a Quantum Design MPMS-XL-5 SQUID magnetometer working in the 2 to 400 K temperature range with an applied magnetic field 0.1 T. Experimental susceptibilities were corrected for diamagnetism of the constituent atoms by the use of Pascal's constants.

Calorimetric measurements were performed using a differential scanning calorimeter Mettler Toledo DSC 821e. Low temperatures were obtained with an aluminium block attached to the sample holder, refrigerated with a flow of of liquid nitrogen gas to avoid water condensation. The measurements were carried out using around 15 mg of polycrystalline samples sealed in aluminium pans with a mechanical crimp. Temperature and heat flow calibrations were made with standard samples of indium by using its melting transition (429.6K, 28.45 J g^{-1}). An overall accuracy of ±0.2K in temperature and ± 2% in the heat capacity is estimated. The uncertainty increases for the determination of the anomalous enthalpy and entropy due to the subtraction of an unknown baseline.

Powder X-ray diffraction measurements were performed on a PANalytical Empyrean X-ray powder diffractometer (monochromatic CuKα radiation) in capillary measurement mode. Due to the spontaneous rehydration of **1(OH)^{Pt}** and **1(OH)^{Pd}**, these samples were prepared by heating the hydrated forms into open capillaries inside an oven at 120ºC for 1 hour and rapidly sealing them to avoid the entering of air

In situ powder X-ray diffraction (PXRD). Temperature and atmosphere dependent measurement were performed in a Malvern PANalytical Empyrean diffractometer equipped with a TTK-600 non-ambient chamber (Anton Paar) with Kapton windows connected to a mass flow controller and bubbler system with N_2 flow. Diffractograms were collected in reflection geometry with a step size of 0.0131° and a counting time of 175 seconds. A PIXcel3D solid-state detector in scanning mode and a Cu anode (Cu $K\alpha_1$ = 1.5406 Å; Cu $K\alpha_2$ = 1.5444 Å) operating at 45 kV and 40 mA were employed together with 0.02° Soller slits of and ¼ divergence and anti-scatter slits. Powder samples were carefully grinded and loaded into a sample holder inside the TTK-600 non-ambient chamber to be activated in situ by heating at 400 K under N_2 flow. Then, a N_2 current (60 mL/min) was flown through a bubbler containing the specified solvents to create a saturated atmosphere in the chamber.

Single crystal X-ray measurements. Single crystals were mounted on a glass fibre using a viscous hydrocarbon oil to coat the crystal and then transferred directly to the cold nitrogen stream for data

collection. X-ray data were collected on a Supernova diffractometer equipped with a graphitemonochromated Enhance (Mo) X-ray Source (λ = 0.71073 Å). The program CrysAlisPro, Oxford Diffraction Ltd., was used for unit cell determinations and data reduction. Empirical absorption correction was performed using spherical harmonics, implemented in the SCALE3 ABSPACK scaling algorithm. The structures were solved by direct methods using SHELXS-2014 and refined by full matrix least-squares on F^2 using SHELXL-2014 (Sheldrick, G. M. Crystal Structure Refinement with SHELXL. *Acta Crystallogr., Sect. C: Struct. Chem*. 2015, 71, 3−8). Non-hydrogen atoms were refined anisotropically, and hydrogen atoms were placed in calculated positions refined using idealized geometries (riding model) and assigned fixed isotropic displacement parameters.

Adsorption/desorption isotherms. Vapor adsorption measurements were recorded on a Micromeritics 3Flex apparatus at relative pressures up to 1 bar and performed ex situ on **1(OH)^{M}**. Samples were degassed overnight at 150 ºC and 10-6 Torr prior to analysis assuring the presence of the totally desolvated **1(OH)^{M}** compounds. A Micromeritics' ISO Controller was used to keep the temperature constant at 293 K for the H_2O, MeOH or EtOH adsorption measurements.

TGA experiments were carried out with a TA instruments TGA550 device equipped with a Pt/Rh oven (Tmax = 1000°C). The time/solvent dependent TGA experiments were performed by connecting the TGA apparatus to a flow mass controller. Thus, a controlled dry nitrogen flow (60 l/min) was passed through the desired solvent (water, methanol or ethanol) at room pressure and a temperature of 30°C and then the mixture (N_2+solvent vapor) was driven until the TGA chamber where a previously desolvated sample 1M was mounted in a Pt pan.

Figure S1. Thermogravimetric measurements of the as synthesized **1(OH)^{Pt}·H$_2$O** and **1(OH)^{Pd}·H$_2$O** compounds.

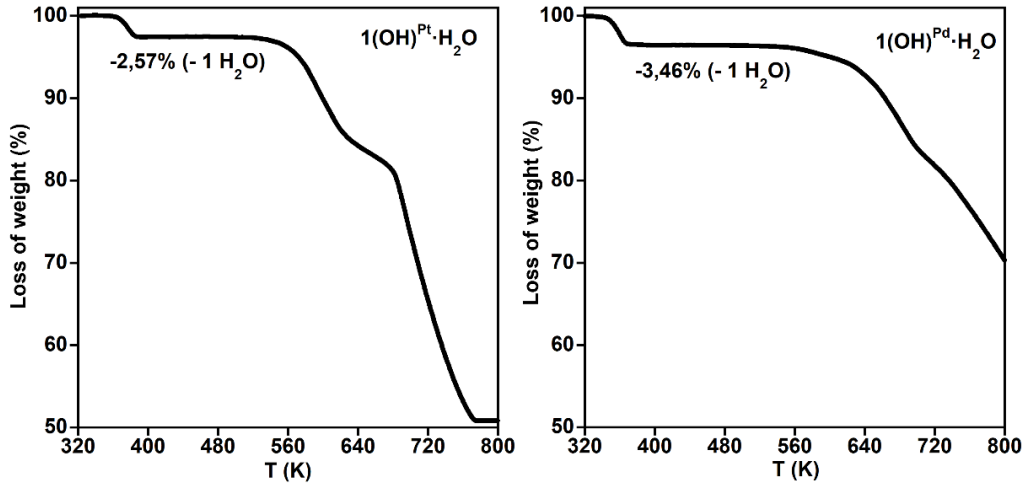

Table S1. Crystal data for compound **1(OH)^{Pt}·H$_2$O** and **1(OH)^{Pt}**.

Sample	**1(OH)^{Pt}·H$_2$O**			**1(OH)^{Pt}**	
Temperature	**120 K**	**230 K**	**260 K**	**120 K**	**260 K**
Empirical formula	$C_{12}H_{11}N_8O_3PtFe$	$C_{12}H_8N_8O_3PtFe$		$C_{12}H_8N_8O_2PtFe$	$C_{12}H_8N_8O_2PtFe$
*M*r	566.23	563.20		547.20	
Crystal system	monoclinic			orthorhombic	
Space group	*C2/m*			*Pnma*	
a (Å)	21.078(4)	21.212(3)	21.669(2)	14.2054(6)	14.6027(8)
b (Å)	7.1279(13)	7.2863(11)	7.4503(7)	7.1095(3)	7.3612(5)
c (Å)	14.407(2)	14.572(2)	14.620(2)	15.3043(7)	15.6975(9)
b (Å)	132.274(8)	132.099(7)	132.408(2)		
V (Å^3)	1601.7(5)	1671.1(5)	1742.8(3)	1545.63(12)	1687.38(18)
Z	4			4	
D_c (mg cm^{-3})	2.348	2.239	2.146	2.352	2.154
F(000)	1068	1056	1056	1024	1024
μ (Mo-K$_\alpha$) (mm^{-1})	9.662	9.260	8.879	10.004	9.163
Crystal size (mm)	0.03x0.30x0.30				
No. of total reflections	2588	2687	3655	4426	4316
No. of reflections [$I>2\sigma(I)$]	2505	2639	3462	3757	3715
R [$I>2\sigma(I)$]	0.0127	0.0175	0.0368	0.0349	0.0287
wR [$I>2\sigma(I)$]	0.0292	0.0429	0.0939	0.0667	0.0513
S	1.094	1.163	1.099	1.156	1.175

$R = \Sigma\,||Fo| - |Fc||\,/\,\Sigma\,|Fo|$; $wR = [\,\Sigma\,[w(Fo^2 - Fc^2)^2]\,/\,\Sigma\,[w(Fo^2)^2]]^{1/2}$.
$w = 1/\,[\sigma^2(Fo^2) + (m\,P)^2 + n\,P]$ where $P = (Fo^2 + 2Fc^2)\,/\,3$;
m = 0.0072 (**120 K**), 0.0084 (**230 K**), 0.0363 (**260 K**), 0.0000 (**120 K (d)**) and 0.0000 (**260 K (d)**);
n = 3.7622 (**120 K**), 10.1726 (**230 K**), 18.5187 (**260 K**), 16.3886 (**120 K (d)**) and 5.7295 (**260 K (d)**)

Table S2. Selected bond lengths [Å] and angles [°] for **1(OH)^{Pt}·H$_2$O** and **1(OH)^{Pt}**.

Sample		**1(OH)^{Pt}·H$_2$O**			**1(OH)^{Pt}**
Temperature	**120 K**	**230 K**	**260 K**	**120 K**	**260 K**
Fe(1)-N(1)	2.015(2)	2.223(4)	2.245(6)		
Fe(1)-N(3)	1.939(2)	2.130(2)	2.125(4)		
Fe(2)-N(4)	1.938(2)	1.939(2)	2.111(4)		
Fe(2)-N(5)	2.005(2)	2.014(3)	2.223(6)		
Pt(1)-C(5)	1.992(2)	1.982(3)	1.975(4)	1.979(3)	1.978(3)
Pt(1)-C(6)	1.989(2)	1.987(3)	1.979(4)	1.981(3)	1.979(3)
Fe(1)-N(1)				1.997(4)	2.209(4)
Fe(1)-N(3)				1.927(3)	2.128(2)
Fe(1)-N(4)				1.932(3)	2.122(2)
Fe(1)-N(5)				2.004(5)	2.260(4)
N(1)-Fe(1)-N(3)	90.59(6)	91.48(10)	91.3(2)		
N(4)-Fe(2)-N(5)	91.38(6)	91.09(9)	90.9(2)		
C(5)-Pt(1)-C(6)	178.84(7)	178.40(10)	179.2(2)	177.88(13)	178.37(12)
N(1)-Fe(1)-N(3)				90.05(12)	89.54(10)
N(1)-Fe(1)-N(4)				91.77(12)	93.42(10)
N(1)-Fe(1)-N(5)				179.1(2)	176.68(14)
N(3)-Fe(1)-N(4)				89.95(12)	90.30(10)
N(3)-Fe(1)-N(5)				89.30(12)	88.10(10)
N(4)-Fe(1)-N(5)				88.88(12)	88.92(11)

Table S3. Crystal data for compound **1(OH)^{Pd}·H$_2$O** and **1(OH)^{Pd}**.

Sample	**1(OH)^{Pd}·H$_2$O**			**1(OH)^{Pd}**	
Temperature	**200 K**	**240 K**	**270 K**	**180 K**	**260 K**
Empirical formula	$C_{12}H_9N_8O_3PdFe$	$C_{12}H_8N_8O_3PdFe$	$C_{12}H_9N_8O_3PdFe$	$C_{12}H_{10}N_8O_2PdFe$	$C_{12}H_8N_8O_2PdFe$
*M*r	475.52	474.51	475.52	460.53	458.51
Crystal system	monoclinic			orthorhombic	
Space group	*C2/m*			*Pnma*	
a (Å)	21.0937(16)	21.3012(13)	21.491(9)	13.9761(9)	14.2973(5)
b (Å)	7.1552(5)	7.3122(5)	7.501(3)	7.1852(5)	7.4281(3)
c (Å)	14.3204(11)	14.4884(9)	16.009(8)	15.2495(10)	15.6554(5)
b (Å)	132.571(2)	132.618(2)	136.955(14)		
V (Å^3)	1591.7(2)	1660.7(2)	1761.5(14)	1531.4(2)	1662.63(10)
Z	4			4	
D_c (mg cm^{-3})	1.984	1.898	1.793	1.997	1.832
F(000)	932	928	932	904	896
μ (Mo-K$_\alpha$) (mm^{-1})	2.073	1.987	1.873	2.146	1.976
Crystal size (mm)	0.02x0.20x0.30				
No. of total reflections	2138	2209	2795	2044	2012
No. of reflections [$I>2\sigma(I)$]	1893	1984	2284	1648	1670
R [$I>2\sigma(I)$]	0.0677	0.0873	0.0586	0.0335	0.0268
wR [$I>2\sigma(I)$]	0.1705	0.2204	0.1522	0.0654	0.0511
S	1.178	1.252	1.104	1.226	1.235

$R = \Sigma \, ||Fo| - |Fc|| \, / \, \Sigma \, |Fo|$; $wR = [\, \Sigma \, [w(Fo^2 - Fc^2)^2] \, / \, \Sigma \, [w(Fo^2)^2]]^{1/2}$.
$w = 1/ \, [\sigma^2(Fo^2) + (m \, P)^2 + n \, P]$ where $P = (Fo^2 + 2Fc^2) \, / \, 3$;
m = 0.0477 (**200 K**), 0.0234 (**240 K**), 0.0643 (**270 K**), 0.0094 (**180 K (d)**) and 0.0000 (**260 K (d)**);
n = 61.1770 (**200 K**), 124.0986 (**240 K**), 27.4453 (**270 K**), 8.5657 (**180 K (d)**) and 5.5403 (**260 K (d)**)

Table S4. Selected bond lengths [Å] and angles [°] for **1(OH)^{Pd}·H$_2$O** and **1(OH)^{Pd}**.

	1(OH)^{Pd}·H$_2$O			**1(OH)^{Pd}**	
	200 K	**240 K**	**270 K**	**180 K**	**260 K**
Fe(1)-N(1)	2.017(9)	2.25(2)	2.253(8)		
Fe(1)-N(3)	1.939(6)	2.123(9)	2.142(5)		
Fe(2)-N(4)	1.933(6)	1.938(9)	2.131(5)		
Fe(2)-N(5)	1.993(9)	1.988(14)	2.234(7)		
Pd(1)-C(5)	1.993(7)	1.970(10)	2.004(5)	1.989(4)	1.987(3)
Pd(1)-C(6)	1.985(7)	2.000(10)	1.997(5)	1.991(4)	1.988(3)
Fe(1)-N(1)				1.997(5)	2.202(4)
Fe(1)-N(3)				1.938(3)	2.133(3)
Fe(1)-N(4)				1.937(3)	2.123(3)
Fe(1)-N(5)				2.000(5)	2.259(4)
N(1)-Fe(1)-N(3)	91.4(3)	92.8(4)	91.9(2)		
N(4)-Fe(2)-N(5)	90.9(3)	90.7(4)	90.9(2)		
C(5)-Pd(1)-C(6)	179.0(3)	177.8(4)	179.7(2)	177.6(2)	178.07(13)
N(1)-Fe(1)-N(3)				90.00(13)	89.00(11)
N(1)-Fe(1)-N(4)				92.47(13)	94.12(11)
N(1)-Fe(1)-N(5)				177.3(2)	174.3(2)
N(3)-Fe(1)-N(4)				89.40(13)	89.74(11)
N(3)-Fe(1)-N(5)				88.13(13)	86.98(11)
N(4)-Fe(1)-N(5)				89.41(13)	89.88(11)

Figure S2. Fragment of the structure of **1(OH)^{M}·H$_2$O** (M = Pt, Pd) showing the packing of three consecutive bimetallic layers stabilized through π-π interactions (highlighted with green dashed lines).

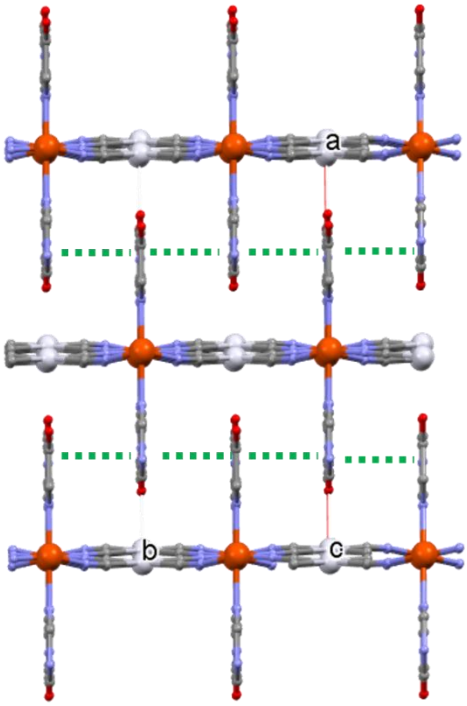

Figure S3. Fragment of the structure of **1(OH)^{M}·H$_2$O** (M = Pt, Pd) showing a perpendicular view to the bimetallic layers where the guest molecules of water, which are disordered by symmetry in two equivalent positions, are located along the 1D channels. The black dashed lines indicate the H-bond stablished between the water molecules.

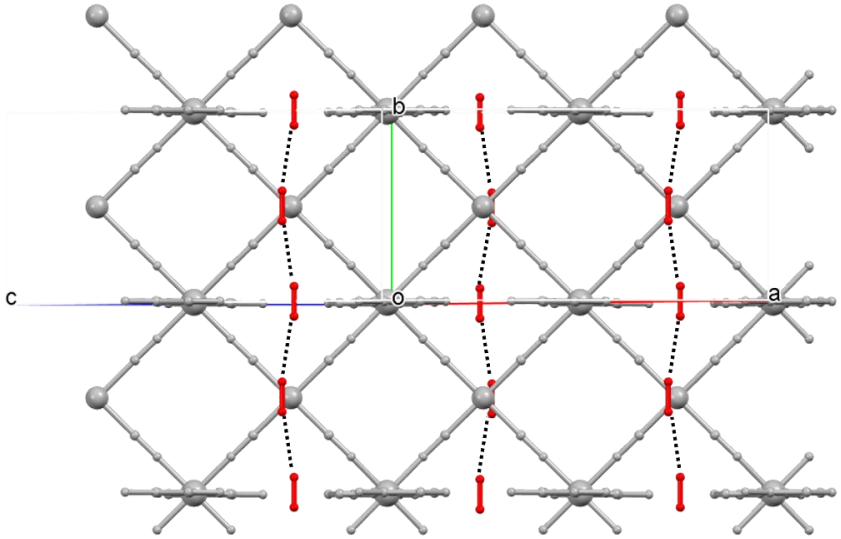

Figure S4. Thermal-dependent magnetic behavior of a) **1(OH)^{Pt}** and b) **1(OH)^{Pd}** and the corresponding amino functionalized derivatives (**1(NH$_2$)^{Pt}** and **1(NH$_2$)^{Pd}**).

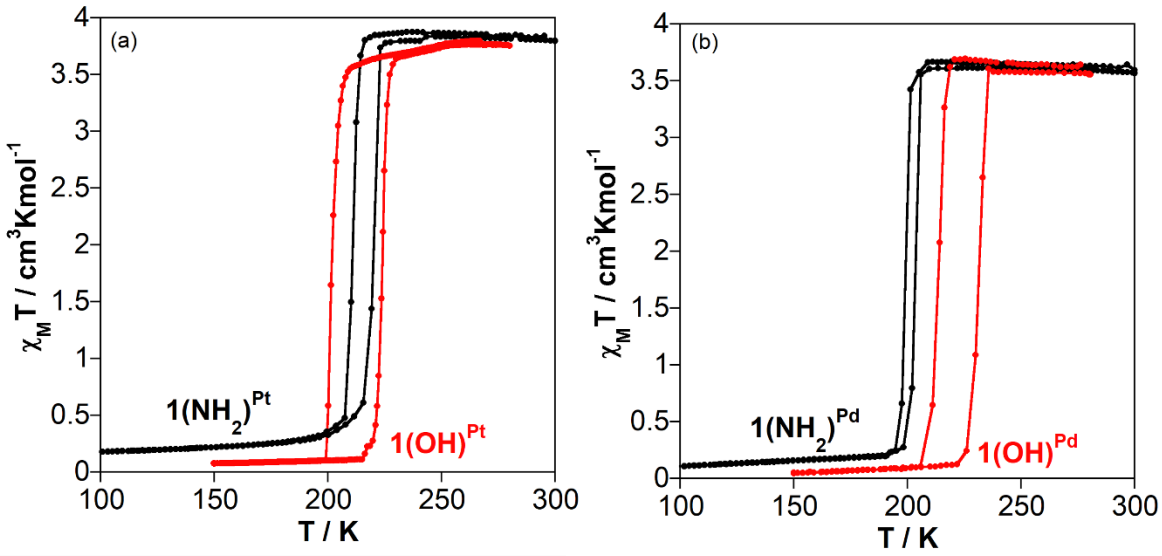

Figure S5. Thermal evolution of the PXRD patterns throughout the **1(OH)^{Pt}·H$_2$O** → **1(OH)^{Pt}** dehydration. The simulated patterns of **1(OH)^{Pt}** and **1(OH)^{Pt}·H$_2$O** are included for comparison.

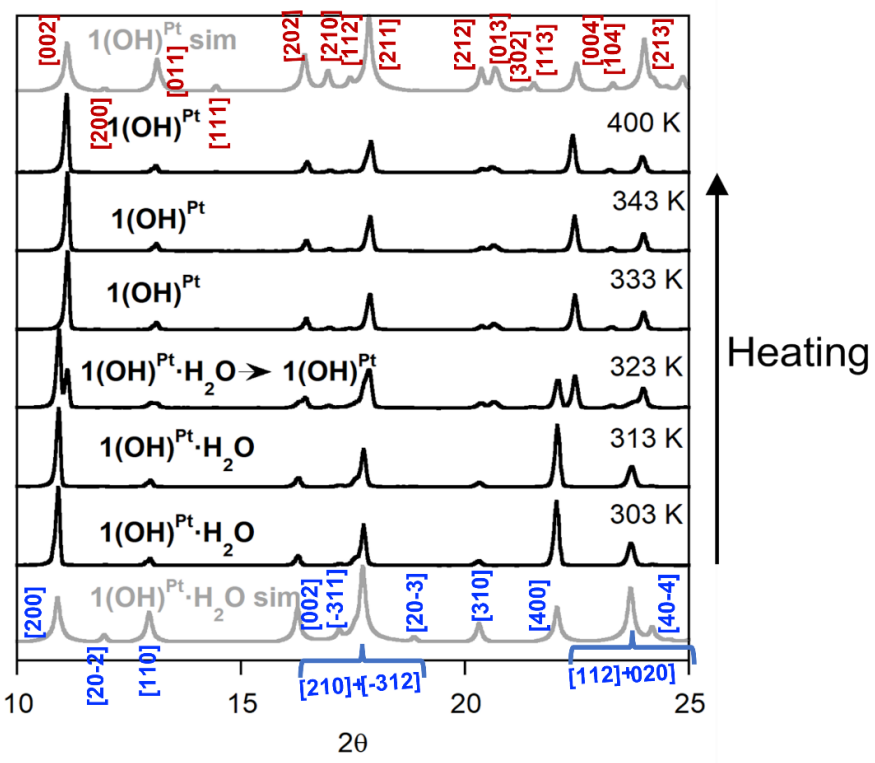

Figure S6. Time dependent PXRD patterns under a dry N_2 flow at 298 K. In these conditions, the **1(OH)^{Pd}·H$_2$O → 1(OH)^{Pd}** dehydration takes place without further heating.

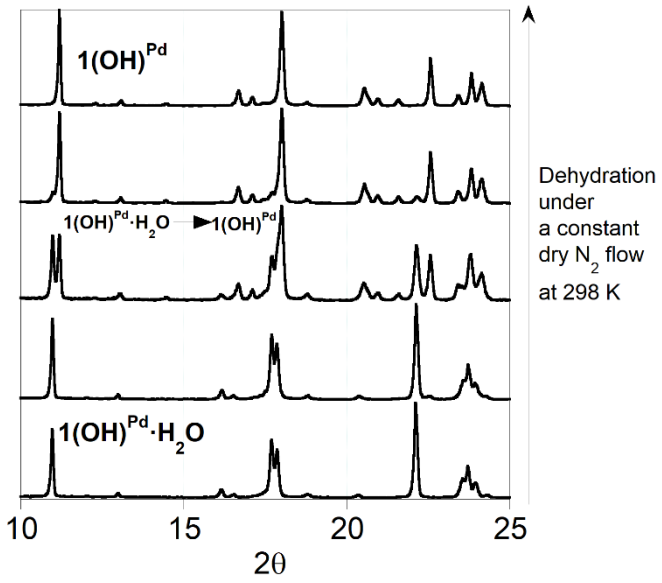

Figure S7. Evolution with time of the PXRD patterns of compound **1(OH)^{Pt}** upon exposure to a N_2 flow saturated with a) water b) methanol and c) ethanol at room temperature.

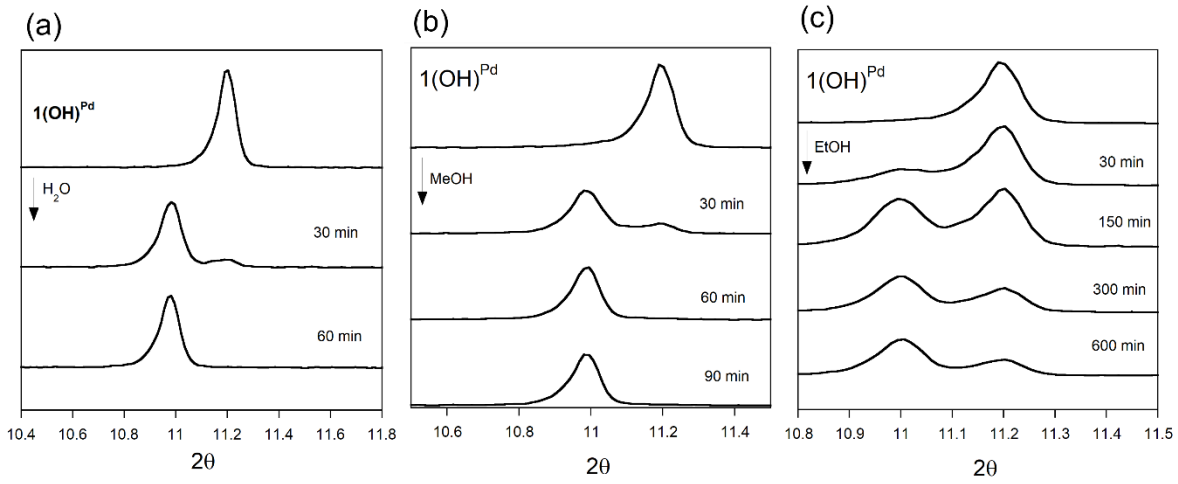

Figure S8. Thermal evolution of the PXRD patterns throughout the **1(OH)^{Pt}·MeOH→1(OH)^{Pt}** and **1(OH)^{Pt}·EtOH→1(OH)^{Pt}** desolvation. The simulated patterns of **1(OH)^{Pt}** and **1(OH)^{Pt}·H_2O** are included for comparison.

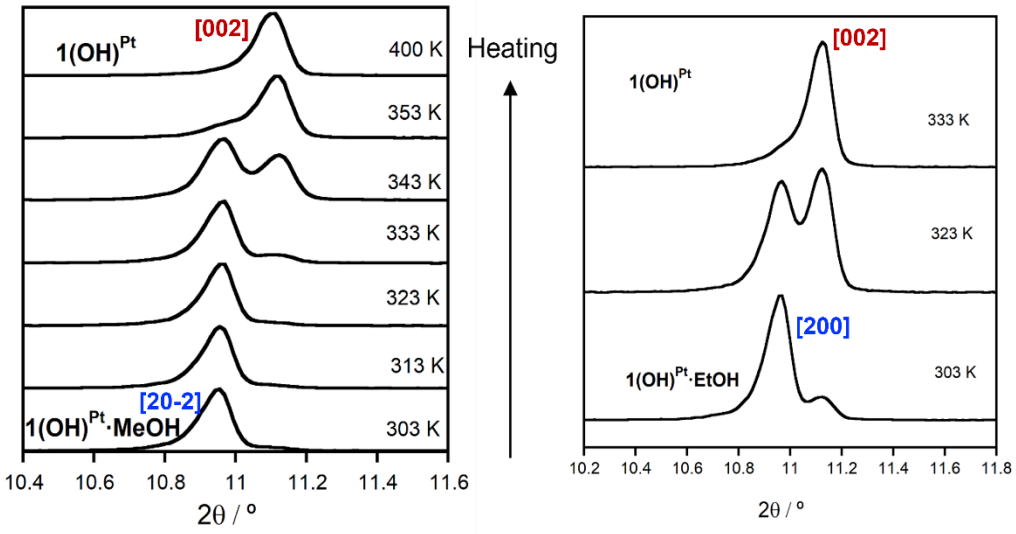

Figure S9. Time dependent evolution of the PXRD patterns throughout the **1(OH)^{Pd}·MeOH→1(OH)^{Pd}** (left) and **1(OH)^{Pd}·EtOH→1(OH)^{Pd}** (right) desolvation. The desorption take place at 298 K without further heating except for **1(OH)^{Pd}·MeOH** which was heated at 400 K to complete the desolvation of methanol.

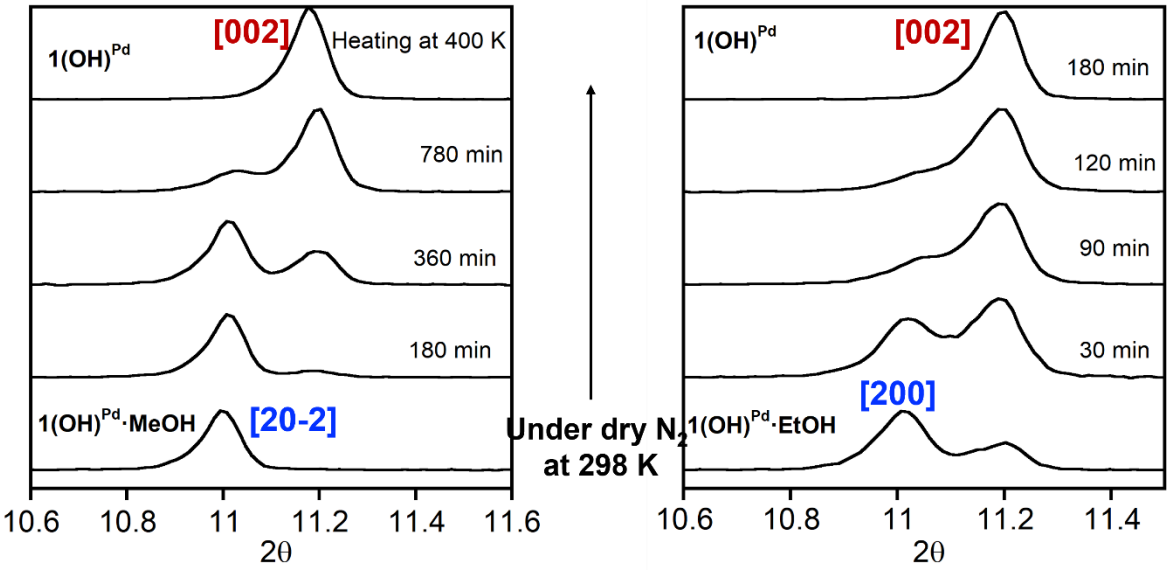

Figure S10. Comparison between the isothermal a) water, b) MeOH and c) EtOH adsorptions of the Pt (red lines) and Pd (blue lines) derivatives analyzed through TGA measurements.

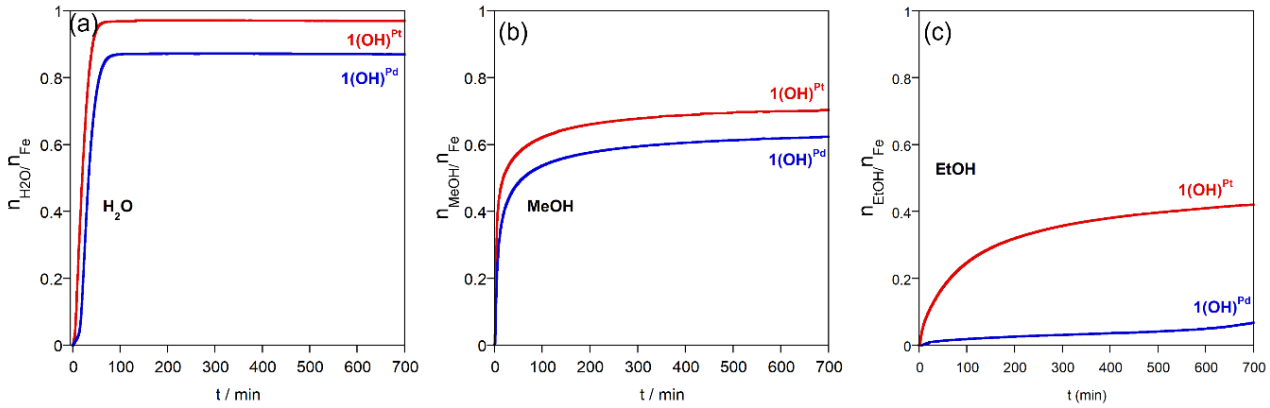

Figure S11. Comparison between the isothermal a,d) water, b,e) MeOH and c,f) EtOH adsorptions carried out through TGA measurements of a,b,c) Pt and d,e,f) Pd derivatives for the hydroxy (red lines) and amine (blue lines) functionalized compounds.

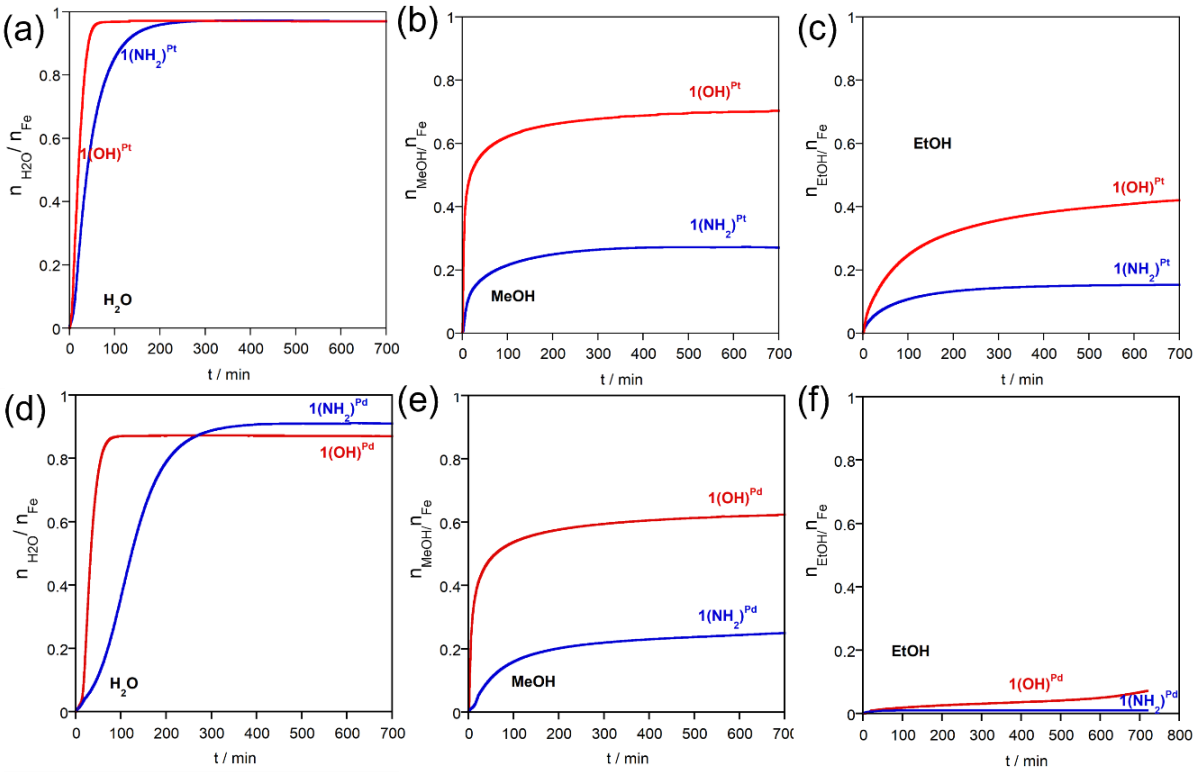

Figure S12. TGA carried out on a,c) **1(OH)^{Pt}**, b,c) **1(OH)^{Pd}** after being immersed in a,b) methanol and c,d) ethanol for 3 days. **Table S5.** Crystal data for compound **1(OH)^{Pt}·0.5MeOH**.

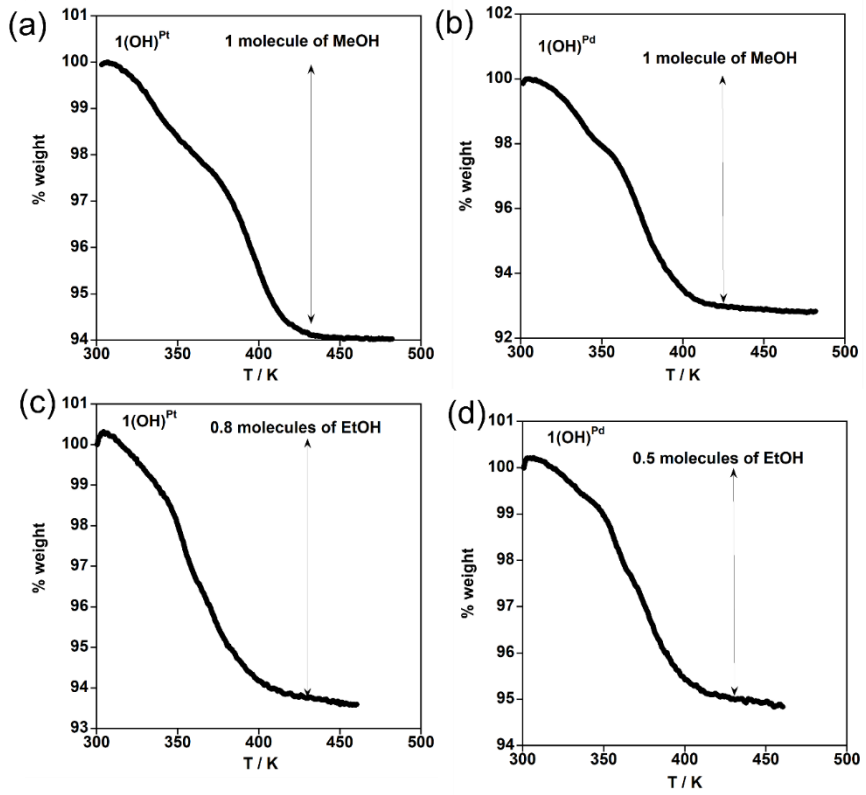

Temperature	**120 K**	**160 K**	**215 K**	**260 K**
Empirical formula	$C_{12.5}H_{10}N_8O_{2.5}PtFe$	$C_{12.5}H_8N_8O_{2.5}PtFe$		
*M*r	563.22	561.21		
Crystal system	monoclinic			
Space group	*C2/m*			
a (Å)	21.2206(10)	21.265(4)	21.567(2)	21.655(3)
b (Å)	7.11020(10)	7.2848(3)	7.3471(2)	7.4564(3)
c (Å)	15.5704(7)	15.680(3)	14.6537(14)	15.983(2)
β (Å)	137.204(9)	136.70(3)	132.69(2)	137.26(3)
V (Å^3)	1596.1(2)	1665.8(8)	1706.7(4)	1751.4(7)
Z	4			
D_c (mg cm^{-3})	2.344	2.238	2.184	2.128
F(000)	1060	1052	1052	1052
μ (Mo-K$_\alpha$) (mm^{-1})	9.693	9.287	9.064	8.833
Crystal size (mm)	0.05x0.15x0.15			
No. of total reflections	2231	2234	2257	2452
No. of reflections [$I>2\sigma(I)$]	2125	2181	2225	2252
R [$I>2\sigma(I)$]	0.0462	0.1138	0.0797	0.0484
wR [$I>2\sigma(I)$]	0.1062	0.2629	0.2014	0.1158
S	1.139	1.382	1.456	1.066

$R = \Sigma \, ||Fo| - |Fc|| \, / \, \Sigma \, |Fo|$; $wR = [\, \Sigma \, [w(Fo^2 - Fc^2)^2] \, / \, \Sigma \, [w(Fo^2)^2]]^{1/2}$.
$w = 1/ \, [\sigma^2(Fo^2) + (m \, P)^2 + n \, P]$ where $P = (Fo^2 + 2Fc^2) \, / \, 3$;
m = 0.0337 (**120 K**), 0.0000 (**160 K**), 0.0001 (**215 K**), and 0.0439 (**260 K**);
n = 80.0706 (**120 K**), 498.4065(**160 K**), 225.6055 (**215 K**), and 78.6952 (**260 K**)

Table S6. Selected bond lengths [Å] and angles [°] for **1(OH)^{Pt}·0.5MeOH**.

Temperature	**120 K**	**160 K**	**215 K**	**260 K**
Fe(1)-N(1)	2.010(13)	2.13(4)	2.19(3)	2.24(2)
Fe(1)-N(3)	1.943(6)	2.11(2)	2.11(2)	2.145(7)
Fe(2)-N(4)	1.942(6)	1.9553(7)	2.043(14)	2.131(8)
Fe(2)-N(5)	2.006(13)	1.99(3)	2.17(3)	2.23(2)
Pt(1)-C(5)	1.988(7)	1.98(2)	1.97(2)	2.000(9)
Pt(1)-C(6)	1.991(8)	1.98(2)	1.99(2)	2.001(9)
N(1)-Fe(1)-N(3)	91.2(3)	90.7(8)	91.7(8)	91.7(4)
N(4)-Fe(2)-N(5)	91.4(4)	90.0(6)	91.0(8)	91.6(4)
C(5)-Pt(1)-C(6)	178.8(3)	178.1(8)	178.0(7)	178.9(4)

Table S7. Crystal data for compound **1(OH)^{Pt}·0.5EtOH**.

	120 K	**260 K**
Empirical formula	$C_{13}H_6N_8O_{2.5}PtFe$	
*M*r	565.20	
Crystal system	monoclinic	
Space group	*C*2/*m*	
a (Å)	21.123(4)	21.724(2)
b (Å)	7.1448(3)	7.4168(2)
c (Å)	14.419(3)	14.758(2)
β (Å)	132.39(3)	132.57(2)
V (Å^3)	1607.2(7)	1751.1(5)
Z	4	
D_c (mg cm^{-3})	2.336	2.144
F(000)	1056	
μ (Mo-K$_\alpha$) (mm^{-1})	9.627	8.836
Crystal size (mm)	0.05x0.20x0.20	
No. of total reflections	1890	2051
No. of reflections [$I>2\sigma(I)$]	1708	1825
R [$I>2\sigma(I)$]	0.0614	0.0521
wR [$I>2\sigma(I)$]	0.1471	0.1286
S	1.150	1.150

$R = \Sigma \, ||Fo| - |Fc|| \, / \, \Sigma \, |Fo|$; $wR = [\, \Sigma \, [w(Fo^2 - Fc^2)^2] \, / \, \Sigma \, [w(Fo^2)^2]]^{1/2}$.
$w = 1/ \, [\sigma^2(Fo^2) + (m \, P)^2 + n \, P]$ where $P = (Fo^2 + 2Fc^2) \, / \, 3$;
m = 0.0492 (**120 K**), and 0.0561 (**260 K)**;
n = 114.3597 (**120 K**), and 54.7022 (**260 K)**

Table S8. Selected bond lengths [Å] and angles [°] for **1(OH)^{Pt}·0.5EtOH**.

	120 K	**260 K**
Fe(1)-N(1)	2.06(2)	2.2578(8)
Fe(1)-N(3)	1.965(10)	2.130(9)
Fe(2)-N(4)	1.951(10)	2.128(9)
Fe(2)-N(5)	2.03(2)	2.23(2)
Pt(1)-C(5)	1.987(11)	1.982(10)
Pt(1)-C(6)	1.990(12)	1.977(10)
N(1)-Fe(1)-N(3)	91.4(6)	90.4(3)
N(4)-Fe(2)-N(5)	91.1(6)	91.6(6)
C(5)-Pt(1)-C(6)	178.7(5)	179.0(5)

Table S9. Crystal data for compound **1(OH)^{Pd}·0.5MeOH**.

	120 K	**195 K**	**225 K**	**260 K**
Empirical formula	$C_{12.5}H_{10}N_8O_{2.5}PdFe$	$C_{12.5}H_6N_8O_{2.5}PdFe$	$C_{12.5}H_7N_8O_{2.5}PdFe$	$C_{12.5}H_8N_8O_{2.5}PdFe$
*M*r	474.53	470.50	471.51	472.52
Crystal system	monoclinic			
Space group	*C2/m*			
a (Å)	21.068(3)	21.3476(12)	21.386(4)	21.377(5)
b (Å)	7.1391(2)	7.3127(2)	7.3624(4)	7.4740(5)
c (Å)	14.373(2)	15.6544(9)	14.569(3)	15.967(4)
β (Å)	132.50(2)	137.120(11)	132.54(3)	136.88(5)
V (Å^3)	1593.9(5)	1662.9(3)	1690.1(8)	1743.6(12)
Z	4			4
D_c (mg cm^{-3})	1.977	1.879	1.853	1.800
F(000)	932	916	920	924
μ (Mo-K$_\alpha$) (mm^{-1})	2.067	1.981	1.949	1.890
Crystal size (mm)	0.03x0.20x0.25			
No. of total reflections	1848	1935	1914	1985
No. of reflections [$I>2\sigma(I)$]	1762	1888	1813	1660
R [$I>2\sigma(I)$]	0.0794	0.1564	0.1131	0.0708
wR [$I>2\sigma(I)$]	0.1978	0.3495	0.2628	0.2033
S	1.373	1.285	1.314	1.150

$R = \Sigma \, ||Fo| - |Fc|| \, / \, \Sigma \, |Fo|$; $wR = [\, \Sigma \, [w(Fo^2 - Fc^2)^2] \, / \, \Sigma \, [w(Fo^2)^2]]^{1/2}$.
$w = 1/ [\sigma^2(Fo^2) + (m\,P)^2 + n\,P]$ where $P = (Fo^2 + 2Fc^2) / 3$;
m = 0.0441 (1**20 K**), 0.0000 (**195 K**), 0.0001 (**225 K**), and 0.1022 (**260 K)**;
n = 129.8175 (**120 K**), 415.4154 (**195 K**), 189.2513 (**225 K**), and 33.7069 (**260 K)**

Table S10. Selected bond lengths [Å] and angles [°] for **1(OH)^{Pd}·0.5MeOH**.

	120 K	195 K	225 K	260 K
Fe(1)-N(1)	2.01(2)	2.17(3)	2.19(3)	2.235(11)
Fe(1)-N(3)	1.938(8)	2.091(14)	2.094(14)	2.127(8)
Fe(2)-N(4)	1.935(7)	1.974(14)	2.019(11)	2.119(7)
Fe(2)-N(5)	2.00(2)	2.05(3)	2.09(3)	2.220(11)
Pd(1)-C(5)	1.990(9)	2.00(2)	2.00(2)	1.975(9)
Pd(1)-C(6)	1.988(9)	1.98(2)	1.990(12)	1.978(8)
N(1)-Fe(1)-N(3)	91.4(4)	90.6(6)	91.4(6)	92.2(3)
N(4)-Fe(2)-N(5)	90.9(4)	91.3(6)	91.5(5)	91.4(3)
C(5)-Pd(1)-C(6)	178.6(4)	178.5(7)	178.3(6)	179.5(3)

Figure S13. Fragment of the structure of **1(OH)^{Pt}·0.5EtOH** showing the atom labels of the asymmetric unit cell.

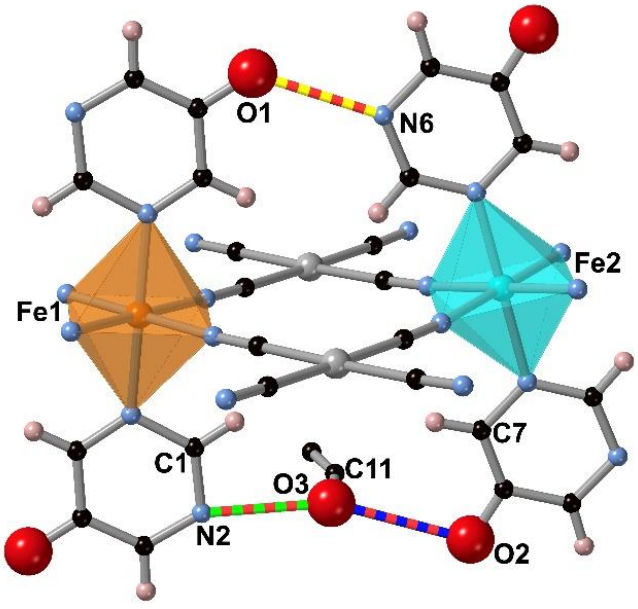

Figure S14. Fragment of the structures of **1(NH$_2$)^{Pt}** and **1(OH)^{Pt}** and the corresponding structural parameters at 260 and 120 K.

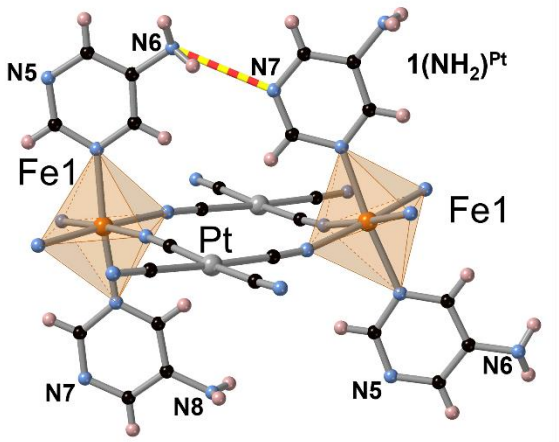

1(NH$_2$)^{Pt}	260 K	120 K
Angle between equatorial planes		
Fe1(N3/N4)$_4$-Pt(C9/C10)$_4$	9.936	3.274
Fe1'(N3/N4)$_4$-Pt(C9/C10)$_4$	24.460	12.088
Fe1(N3N4)$_4$- Fe1'(N3N4)$_4$	14.525	8.813
H-bonding		
N6(H6)···N7	3.023	3.008

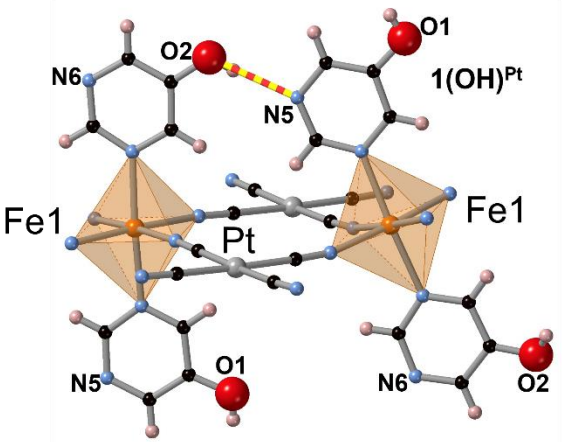

1(OH)^{Pt}	260 K	120 K
Angle between equatorial planes		
Fe1(N3/N4)$_4$-Pt(C9/C10)$_4$	6.045	3.261
Fe1'(N3/N4)$_4$-Pt(C9/C10)$_4$	23.959	18.776
Fe1(N3N4)$_4$- Fe1'(N3N4)$_4$	17.914	15.516
H-bonding		
O2(H2)···N5	2.745	2.730

Figure S15. Fragment of the structures of **1(NH$_2$)^{Pt}·H$_2$O** and **1(OH)^{Pt}·H$_2$O** and the corresponding octahedral distortion parameters in the HS-HS, HS-LS and LS-LS states.

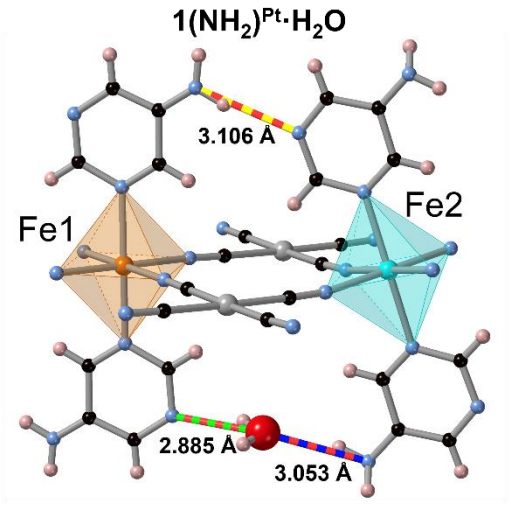

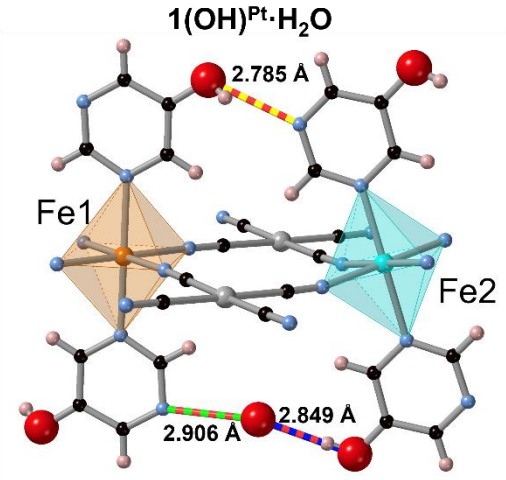

	Fe1				Fe2			
T/K	**Θ/°**	**Σ/°**	**<Fe-N>**	**State**	**Θ/°**	**Σ/°**	**<Fe-N>**	**State**
260	22	11.6	2.159	HS	39	22.8	2.164	HS
187	21	12.0	1.965	LS	33	25.2	2.140	HS
100	17	14.0	1.948	LS	29	13.2	1.955	LS

	Fe1				Fe2			
T/K	**Θ/°**	**Σ/°**	**<Fe-N>**	**State**	**Θ/°**	**Σ/°**	**<Fe-N>**	**State**
260	34	14.2	2.166	HS	28	7.8	2.148	HS
230	33	20.6	2.161	HS	21	13.4	1.964	LS
120	21	7.5	1.964	LS	23	11.2	1.953	LS

Figure S16. Fragment of the structures of **1(NH$_2$)^{Pt}·0.5MeOH** and **1(OH)^{Pt}·0.5MeOH** and corresponding structural parameters at each measurement temperature.

1(NH$_2$)^{Pt}·0.5MeOH

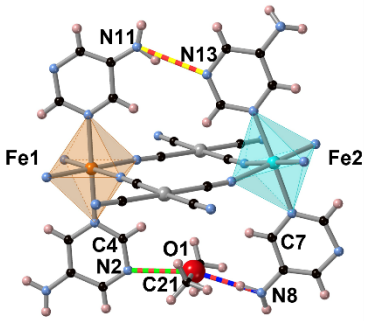

1(NH$_2$)^{Pt}·0.5MeOH	260 K	120 K
Angle between equatorial planes		
Fe1(N4)$_4$-Pt(C5/C6)$_4$	2.085	1.144
Fe2(N5)$_4$-Pt(C5/C6)$_4$	17.473	16.269
Fe1(N4)$_4$- Fe2(N5)$_4$	15.388	15.125
H-bonding		
N11pymFe1···N13pymFe2	3.015	3.007
N2pymFe1···O1MeOH	2.724	2.736
N8···O1MeOH	2.900	2.830
Short contacts C(MeOH)···pymFe1/Fe2		
O1MeOH···C4pymFe1	3.171	3.140
O1(MeOH)···C7pymFe2	3.603	3.605
C21(MeOH)···C4pymFe1	3.458	3.381
C21(MeOH)···N2pymFe1	3.029	3.059
C21(MeOH)···N8pymFe2	3.179	3.205

1(OH)^{Pt}·0.5MeOH

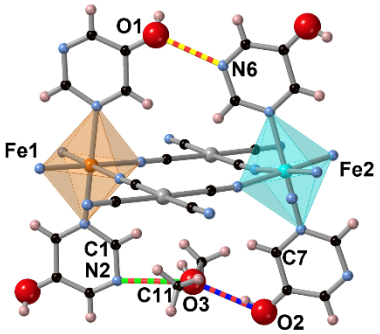

1(OH)^{Pt}·0.5MeOH	260 K	215 K	160 K	120 K
Angle between equatorial planes				
Fe1(N3)$_4$-Pt(C5/C6)$_4$	3.099	4.012	3.365	4.792
Fe2(N4)$_4$-Pt(C5/C6)$_4$	14.309	13.502	13.894	11.586
Fe1(N3)$_4$- Fe2(N4)$_4$	17.409	17.514	17.259	16.378
H-bonding				
O1(pymFe1)**H**···N6(pymFe2)	2.735	2.811	2.749	2.669
N2(pymFe1)···**H**(O3MeOH)	2.904	2.948	2.928	2.745
O2(pymFe2)**H**···(O3MeOH)	2.865	2.815	2.714	2.778
Short contacts				
O3MeOH··· C1pymFe1	3.204	3.170	3.156	3.073
O3MeOH··· C7pymFe2	3.406	3.389	3.333	3.249
C11/14(MeOH)···C1pymFe1	3.326	3.388	3.310	3.259
C11/14(MeOH)···O2pymFe2	3.336	3.196	3.196	3.195
C11(MeOH)···N2pymFe1	3.114	3.262	3.178	3.011

Figure S17. SCO properties of compounds **1(NH$_2$)^{Pt}·0.5MeOH** (extracted from reference 28 in the main text) and **1(OH)^{Pt}·0.5MeOH**.